# A Cobalt Mimochrome for Photochemical Hydrogen

## **Evolution from Neutral Water**

Emily H. Edwards†a, Jennifer M. Le†a, Alison A. Salamatiana, Noelle L. Pelusoa, Linda Leoneb, Angela Lombardib, and Kara L. Brena

<sup>a</sup>Department of Chemistry, University of Rochester, 120 Trustee Rd., Rochester, NY 14627-0216, U.S.A.

<sup>b</sup>Department of Chemical Sciences, University of Naples Federico II, Complesso Universitario Monte S. Angelo, via Cintia 45, 80126 Naples, Italy.

†Authors contributed equally

Additional author emails:

E.H.E.: eedward6@ur.rochester.edu

J.M.L.: p.h.m.le@rug.nl

A.A.S.: asalamat@ur.rochester.edu

N.L.P.: npeluso2@u.rochester.edu

L.L.: linda.leone@unina.it

A.L.: alombard@unina.it

#### **Abstract**

A system for visible light-driven hydrogen production from water is reported. This system makes use of a synthetic mini-enzyme known as a mimochrome (CoMC6\*a) consisting of a cobalt deuteroporphyrin and two attached peptides as a catalyst, [Ru(bpy)<sub>3</sub>]<sup>2+</sup> (bpy = 2,2'-bipyridine) as a photosensitizer, and ascorbic acid as a sacrificial electron donor. The system achieves turnover numbers (TONs) up to 10,000 with respect to catalyst and optimal activity at pH 7. Comparison with related systems shows that CoMC6\*a maintains the advantages of biomolecular catalysts, while exceeding other cobalt porphyrins in terms of total TON and longevity of catalysis. Herein, we lay groundwork for future study, where the synthetic nature of CoMC6\*a will provide a unique opportunity to tailor proton reduction chemistry and expand to new reactivity.

## **Keywords**

Artificial photosynthesis

Biomolecular catalyst

Cobalt catalysis

De novo design

Hydrogen evolution

Photocatalysis

## **Abbreviations**

bpy: bipyridine

**Co-cyt** *b*<sub>562</sub>: Cobalt cytochrome *b*<sub>562</sub> (M7A mutant)

CoGGH: cobalt glycine-glycine-histidine

CoMC6\*a: cobalt mimochrome VI\*a

CoMyo: cobalt protoporphyrin IX substituted into apomyoglobin

**CoMP11-Ac:** acetylated cobalt microperoxidase-11

**CoP:** cobalt *meso*-tetrakis(1-methylpyridinium-4-yl) porphyrin

**CoTPPS:** cobalt *meso*-tetrakis(p-sulfonylphenyl)

dmg: dimethylglyoxime

py: pyridine

**Ru**<sup>2+</sup>: ruthenium(II) trisbipyridine

**SHE:** standard hydrogen electrode

**TON:** turnover number

**TOF:** turnover frequency

#### 1. Introduction

Light-driven chemistry has been an active area of research for decades, but has experienced renewed interest in recent years [1]. A compelling motive for studying light-driven chemistry currently in the spotlight is the development of renewable energy resources [2-4]. While the sun is a potent energy source, using its energy to catalyze reactions that produce a chemical fuel – an artificial photosynthetic process – is not trivial [5]. Splitting water with energy from light is one of the long sought-after goals of artificial photosynthesis [6, 7]. However, success demands finding practical, economical, and environmentally friendly ways to couple water oxidation and proton reduction [7-9]. Numerous challenges contained in the coupling process have resulted in the oxidative and reductive processes being studied in separate model systems. Here, we study the proton reduction half reaction, which can be used to produce the carbon-free fuel hydrogen [10].

Nature's catalysts for proton reduction, hydrogenases, use earth abundant iron and/or nickel [11]. While some studies have evolved hydrogenase enzymes to control reactivity and decrease oxygen sensitivity, they are still impacted by a low density of active sites [12, 13]. Inspired by hydrogenase, numerous molecular catalysts containing first-row transition metals such as iron, nickel, and cobalt, have been developed [14-17]. Although cobalt is not utilized by hydrogenase enzymes, cobalt-containing catalysts have become some of the most prominent molecular candidates [18-20]. A variety of glyoxime-[21-27], dithiolene-[28, 29], macrocyclic-[30-33], and polypyridyl- [34-41] based scaffolds for cobalt catalysts have been vetted. While molecular systems are often more easily tailored through synthesis [9, 42], the ability of hydrogenase enzymes to reversibly catalyze the proton reduction reaction is connected to their highly evolved protein structures [43, 44]. Emergent biomolecular systems aim to benefit from the interface of molecular catalysis and enzymatic catalysis.

Biomolecular catalysts possess a range of advantages [3, 45], but examples of biomolecular cobalt catalysts for proton reduction remain limited. Some work has interfaced established molecular catalysts with protein scaffolds. Cobalt bis-glyoxime derivatives have been attached to sperm whale myoglobin, heme oxygenase, and ferredoxin [26, 46, 47]. While a protein scaffold enhances the water solubility of these catalysts, the turnover numbers (TONs) observed in these studies were limited. Another catalyst, CoMyo, incorporated cobalt protoporphyrin IX into a sperm whale myoglobin scaffold [48]. This work demonstrated the versatility a protein scaffold brings, allowing for mutations at desired residues near the active site. Unlike the case of the cobalt bisglyoxime catalysts, the scaffold provided an enhancement in TON compared to the free porphyrin. Alongside these works, we incorporated a simple tripeptide cobalt catalyst, cobalt glycine-glycinehystidine (CoGGH) into a photochemical system [49]. In addition, the photochemical activity of acetylated cobalt microperoxidase-11 (CoMP11-Ac), a cobalt porphyrin covalently bound to an 11-amino acid peptide, was recently evaluated [50]. The latter two works pointed to the propensity of biomolecular catalysts to achieve high activity near neutral pH in photochemical systems. Here, we follow up on these works with the use of cobalt mimochrome VI\*a (CoMC6\*a), a mini-protein with a larger peptide scaffold than CoMP11-Ac.

The mimochrome minienzyme has been tailored for a variety of applications [51, 52] Incorporation of a catalytic unit into a protein scaffold requires that the scaffold is suited to fit the steric requirements of the catalyst, that the protein retains the desired fold when the catalyst is bound, and that the catalyst can bind to the scaffold strongly without coordinatively saturating the active site. The synthetic nature of the mimochrome allows it to be tailored to meet these requisites [51]. CoMC6\*a contains a cobalt deuteroporphyrin active site, an analog of protoporphyrin IX lacking vinyl side chains. Its peptide scaffold consists of a proximal tetradecapeptide and a distal

decapeptide chain, each covalently bound to the deuteroporphyrin propionic acid moieties. The proximal peptide provides axial histidine ligation for the metal center (Fig. 1). CoMC6\*a has been characterized for its proton reduction activity electrochemically in previous work [53, 54]. In the electrocatalytic work, CoMC6\*a was compared to CoMP11-Ac directly [53], and here we expand that comparison to a photochemical system. When paired with [Ru(bpy)<sub>3</sub>]Cl<sub>2</sub> (bpy = 2,2'-bipyridine) (Ru<sup>2+</sup>) and ascorbate (Fig. 1), we show that CoMC6\*a facilitates TONs over 10,000 with respect to catalyst, exceeding other cobalt porphyrin catalysts in photochemical systems. The cobalt mimochrome shows its best activity near neutral pH, and is stable during photocatalysis. CoMC6\*a maintains the benefits of other biomolecular scaffolds, but presents the advantage of a completely tailorable mini enzyme for future photochemical systems.

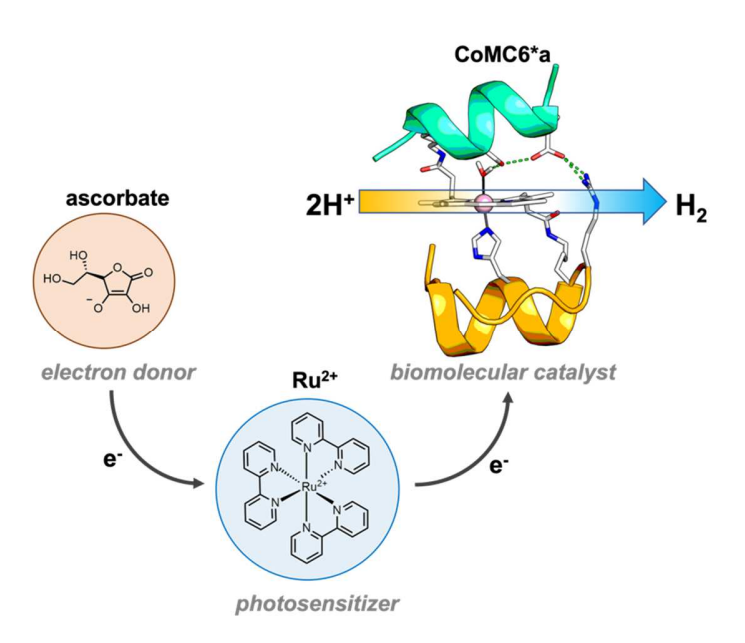


**Fig. 1.** Schematic of system for photochemical H<sub>2</sub> production showing the structure of the CoMC6\*a catalyst.

#### 2. Experimental

#### 2.1. Materials

L-ascorbic acid (Fisher Scientific), [Ru(bpy)<sub>3</sub>]Cl<sub>2</sub>(Sigma Aldrich), and piperazine (Sigma-Aldrich) were purchased and used without further purification.

#### 2.2 CoMC6\*a preparation and purification

CoMC6\*a was prepared and purified as previously described [53, 55]. Stock solutions of CoMC6\*a are stored at -80 °C.

## 2.3 Hydrogen-evolution experiments for total hydrogen evolution

Fresh stock solutions of ascorbic acid and [Ru(bpy)<sub>3</sub>]Cl<sub>2</sub> were prepared in 1 M piperazine buffer (pH 6.5) in doubly deionized water. The solutions were diluted to the desired concentration of each component with 1 M piperazine buffer (pH 6.5) to yield 1 mL total solutions. For studies of pH dependence, 1 M piperazine solutions were prepared at pH values ranging from 2.5 – 10.5 and used to prepare 1-mL solutions. Solution pH was adjusted as required to the desired pH with small volumes of NaOH or HCl. The pH was measured before and after each experiment and remained within ± 0.1 pH units. A Shimadzu 8452 UV-vis absorption spectrometer was used to collect absorption spectra before and after the experiment at 50x dilution. For photochemical experiments, the 1-mL solutions were housed in 2-mL vials with a headspace of 1 mL. The vials were sealed with gas-tight septa and purged with 79.31%/20.69% N<sub>2</sub>/CH<sub>4</sub> (Airgas) as an internal standard for 10 minutes. All vials were placed in a custom-built temperature-controlled block connected to Thermotek circulating water bath at 15 °C and illuminated from below by 0.20 W blue (447.5 nm) light-emitting diodes (Philips LumiLED Luxeon Star Hex 700 mA LEDS mounted on a 20 mm starshaped CoolBases). A L30A thermal sensor and a Nova II power meter (Ophir-Spiricon LLC) were used to measure each LED individually before and after the

experiment. The block was mounted on a Thermo-Scientific MaxQ orbital shaker which allowed for continuous mixing at 100 RPM.

## 2.4 Hydrogen-evolution experiments for initial rates

Buffer stock solutions were prepared as described in section 2.3. For photochemical experiments used to measure initial rates and hydrogen evolution over time, 5-mL solutions were prepared, each in a 41-mL vial with a headspace of 36 mL. The vials were sealed with gas-tight septa and purged with 79.31%/20.69% N<sub>2</sub>/CH<sub>4</sub> (Airgas) as an internal standard for 15 minutes. As described above, all vials were placed in a custom-built temperature-controlled block connected to Thermotek circulating water bath at 15 °C and illuminated from below by 0.20 W blue (447.5 nm) light-emitting diodes (Philips LumiLED Luxeon Star Hex 700 mA LEDS mounted on a 20 mm starshaped CoolBases). A L30A thermal sensor and a Nova II power meter (Ophir-Spiricon LLC) were used to measure each LED individually before and after the experiment. The block was mounted on a Thermo-Scientific MaxQ orbital shaker which allowed for continuous mixing at 100 RPM.

## 2.5 Quantification of hydrogen

A Shimadzu GC-2014 gas chromatograph (GC) with a thermal conductivity detector and a 5-Å molecular sieve column (30 m  $\times$  0.53 mm) was used to monitor  $H_2$  production. A 25- $\mu$ L sample of the headspace gas was withdrawn with a gastight syringe (Hamilton) from each sample and injected into the GC for analysis. Quantification was based on a calibration curve of the ratio  $H_2/CH_4$  vs. volume of  $H_2$  constructed by injecting known volumes (see SI for additional information).

#### 2.6 Luminescence quenching

Steady-state emission quenching of photoexcited  $[Ru(bpy)_3]^{2+*}$  (\* $Ru^{2+}$ ) by ascorbate (0–0.11 M) or CoMC6\*a (0 – 4  $\mu$ M) was measured using a fluorometer (Acton Research).  $[Ru(bpy)_3]^{2+}$  ( $Ru^{2+}$ ) at 50  $\mu$ M concentration in 1 M piperazine, pH 6.5, was excited at 460 nm, and the emission was monitored between 530 and 800 nm with a slit width of 5 mm and integration time of 500 ms. The observed quenching behavior was fit to the Stern-Volmer equation:  $I_0/I = K_{SV}[Q] + 1$  where  $I_0$  and I describe the maximum fluorescence intensity in the absence and presence of quencher, respectively. [Q] is the concentration of the quencher and  $K_{SV}$  is the Stern-Volmer constant. Quenching rate constants ( $k_q$ ) were calculated by using the triplet state lifetime of 620 ns reported for \* $Ru^{2+}$  in water [56].

#### 3. Results and Discussion

## 3.1 Photoinitiation of reaction

While there are many routes to light-driven catalysis, model molecular systems benefit from simplicity. Typically, three components are utilized [57, 58]. A photosensitizer absorbs light and initiates charge separation, a catalyst carries out the desired reaction, and an electron donor sustains the reaction (Fig. 1). Pairing a catalyst with a well-studied photosensitizer and electron donor is a valuable way to characterize a catalyst. Ruthenium (tris)bipyridine ( $\mathbf{Ru^{2+}}$ ) has served as a foundational photosensitizer across many works [24, 30, 32, 49, 50, 59-61]. Commonly,  $\mathbf{Ru^{2+}}$  is paired with aqueous electron donor ascorbic acid. Monoprotonated ascorbate, with pK<sub>a</sub> values of 4.1 and 11.8, serves as the primary electron-donating species [60, 62]. Thus, a light-driven system consisting of  $\mathbf{Ru^{2+}}$  as a photosensitizer, ascorbate as the electron donor, and CoMC6\*a as the

catalyst was chosen for study herein. Prior to initiation of photochemical experiments, the catalyst is stable as Co(III)MC6\*a, and is not reduced in the presence of ascorbate (Fig. S1). Blue (447.5 nm) LEDs were used as a light source, as this wavelength is close to the **Ru**<sup>2+</sup> absorbance maximum and in a region of minimal absorbance for Co(III)MC6\*a (Fig. 2A). Irradiation of a solution of Co(III)MC6\*a and **Ru**<sup>2+</sup> leads to reduction of the catalyst to Co(II)MC6\*a (Fig. S2). With all three components (ascorbate, catalyst, **Ru**<sup>2+</sup>) present, hydrogen evolution begins upon irradiation (Fig. 2B). As previously reported, **Ru**<sup>2+</sup> and ascorbate produce some hydrogen when irradiated in the absence of catalyst, but all three components are necessary to maximize hydrogen evolution (Fig. S3).

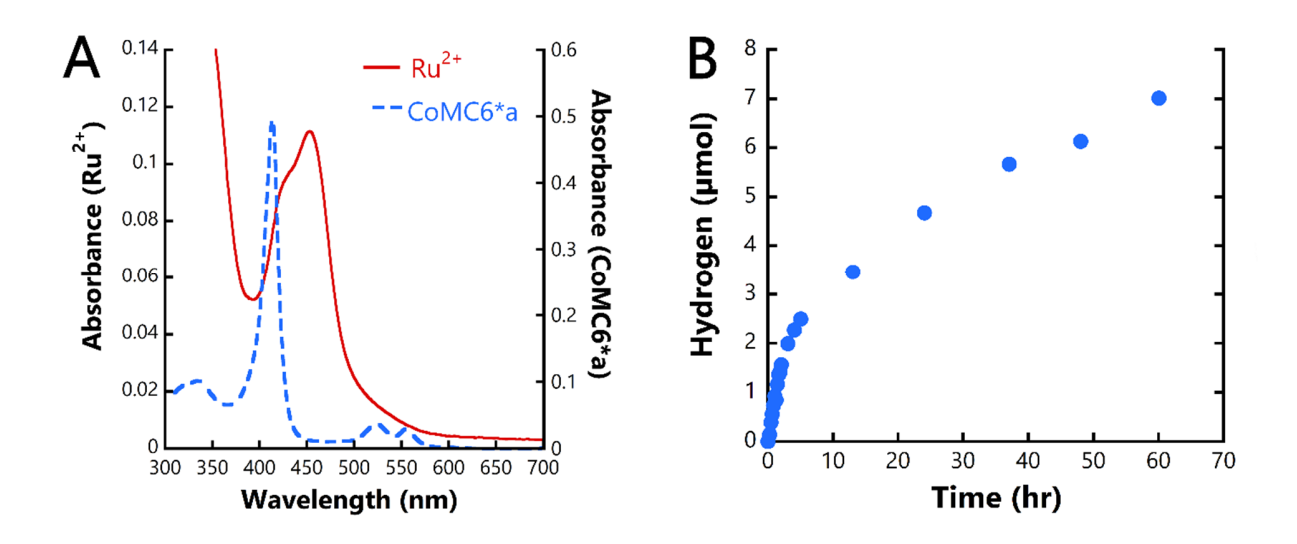


**Fig. 2.** A: The absorbance spectra of  $\mathbf{Ru^{2+}}$  (8  $\mu$ M) and Co(III)MC6\*a (1  $\mu$ M). B: A representative trial demonstrating hydrogen evolved when all three components (sensitizer, catalyst, ascorbate) are present: 400  $\mu$ M  $\mathbf{Ru^{2+}}$ , 1.0  $\mu$ M CoMC6\*a, and 100 mM ascorbic acid in 1 M piperazine buffer, pH 6.5, 5 mL sample, with blue (447.5 nm) LED illumination.

Steady-state luminescence quenching can be used to evaluate the interaction between donor, sensitizer, and catalyst. In particular, it can be discerned whether an oxidative or reductive quenching pathway may initiate the observed catalysis (Fig. S4) [63, 64]. Ascorbate is a wellknown quencher of \*Ru<sup>2+</sup>. Quenching by ascorbic acid under experimental conditions yields a quenching rate constant of 1.8 x 10<sup>7</sup> M<sup>-1</sup>s<sup>-1</sup>, consistent with literature values under similar conditions [30, 32, 36, 49, 50] (Fig. S5). In contrast, quenching by the catalyst, Co(III)MC6\*a, yields a higher rate constant of 1.1 x 10<sup>11</sup> M<sup>-1</sup>s<sup>-1</sup> (Fig. S6). Under concentrations relevant to photochemical conditions, the high concentration of ascorbate (100 mM) relative to CoMC6\*a (1 μM) yields quenching rate constants of 1.8 x 10<sup>6</sup> s<sup>-1</sup> and 1.1 x 10<sup>5</sup> s<sup>-1</sup>, respectively. Since the effective rate constant of quenching by ascorbate is an order of magnitude higher, catalysis is expected to proceed by reductive quenching (Fig. S7), generating a highly reducing Ru<sup>+</sup> species (-1.26 V vs. NHE) [63, 64]. Furthermore, a reductive quenching pathway is expected for catalysis by CoMC6\*a because of its high electrochemical overpotential (approximately 580 mV) for hydrogen evolution, which corresponds to an onset potential of approximately -1.0 V vs. NHE [53, 54]. The rate constant observed for \*Ru<sup>2+</sup> quenching by Co(III)MC6\*a is high, as observed for other biomolecular and cobalt catalysts [28, 36, 37, 49, 50, 61]. The absorption spectra of both Co(III) and Co(II)MC6\*a overlap with the emission spectrum of Ru2+, indicating that energy transfer is possible, which may contribute to the high rate constant (Fig. S8).

Although the practical application of biomolecular catalysts has been purported as challenging due to high overpotentials in electrocatalysis [65, 66], this limitation can be overcome in a photocatalytic system with the correct choice of photosensitizer. We demonstrate here that CoMC6\*a can fuel catalysis via a reductive quenching pathway with  $Ru^{2+}$  as the photosensitizer. Ruthenium dyes are common candidates for dye-sensitized solar cells for solar-to-fuel conversion

[67]. In addition, some of the most promising photosensitizers, nanocrystals, achieve even more reducing potentials than  $Ru^{2+}$  [68, 69]. The size-tunable nature of nanocrystals allows for absorption of longer wavelengths of visible light [70], as does the choice of molecular dye [71, 72]. The reduction potential of sensitizers, through choice of molecular scaffold or engineering of nanocrystals, can be tuned [69, 73]. Uniquely, CoMC6\*a was also demonstrated to have tunable catalytic potentials as a function of solution-dependent protein folding [53] and based on selection of proton donor [54]. The tunability of the CoMC6\*a scaffold may open the possibility to use other less reducing sensitizers, such as molecular dyes, in future work. Biomolecular catalysts like CoMC6\*a provide opportunities to tune overpotential and reactivity on the catalyst end by engineering the active-site microenvironment, which may provide optimum flexibility when paired with a variety of photosensitizers.

#### 3.2. Effects of photosensitizer on hydrogen production

While the choice of  $\mathbf{Ru^{2+}}$  enables catalysis at reducing potentials and allows for comparison to literature, poor photostability of molecular sensitizers is a known limitation of many model systems [34, 74-76]. To better characterize the influence of the sensitizer on overall activity, a variety of sensitizer concentrations were explored. The concentration of  $\mathbf{Ru^{2+}}$  was varied from 0 to 900  $\mu$ M at a constant catalyst concentration of 1.0  $\mu$ M CoMC6\*a. Total hydrogen produced was determined after 48 hours (Fig. 3). In addition, hydrogen production was monitored approximately every 20 minutes during the first two hours of catalysis to measure initial rates (Fig. S9).

The total hydrogen produced increased with increasing [ $\mathbf{Ru^{2+}}$ ], with 900  $\mu$ M producing 10.4  $\mu$ mol  $\pm$  1.0  $\mu$ mol H<sub>2</sub>, corresponding to a TON of (10.4  $\pm$  1.0) x 10<sup>3</sup> with respect to CoMC6\*a concentration (Fig. 3). If the sensitizer concentration is increased beyond 900  $\mu$ M  $\mathbf{Ru^{2+}}$ , the total

hydrogen produced plateaus (Fig. S10). Even in extremely high excess of photosensitizer, there is a significant difference in activity when catalyst is present vs. absent (10.4  $\mu$ mol vs. 0.946  $\mu$ mol, on average, respectively) (Fig. S3). The observed increases in total hydrogen evolved are not merely from increasing sensitizer concentration; the increases rely on catalyst remaining active. The initial rates of catalysis show a linear dependence on the concentration of  $Ru^{2+}$  up to 500  $\mu$ M  $Ru^{2+}$  (Fig. 3), with a minimum of 3.1 x  $10^{-3}$   $\mu$ mol/min at 50  $\mu$ M  $Ru^{2+}$  and a maximum rate of 1.6 x  $10^{-2}$   $\mu$ mol/min at 500  $\mu$ M sensitizer. The initial rates decrease slightly (to a minimum of 1.0 x  $10^{-2}$   $\mu$ mol/min) if the concentration of sensitizer is increased further (Fig. S11).

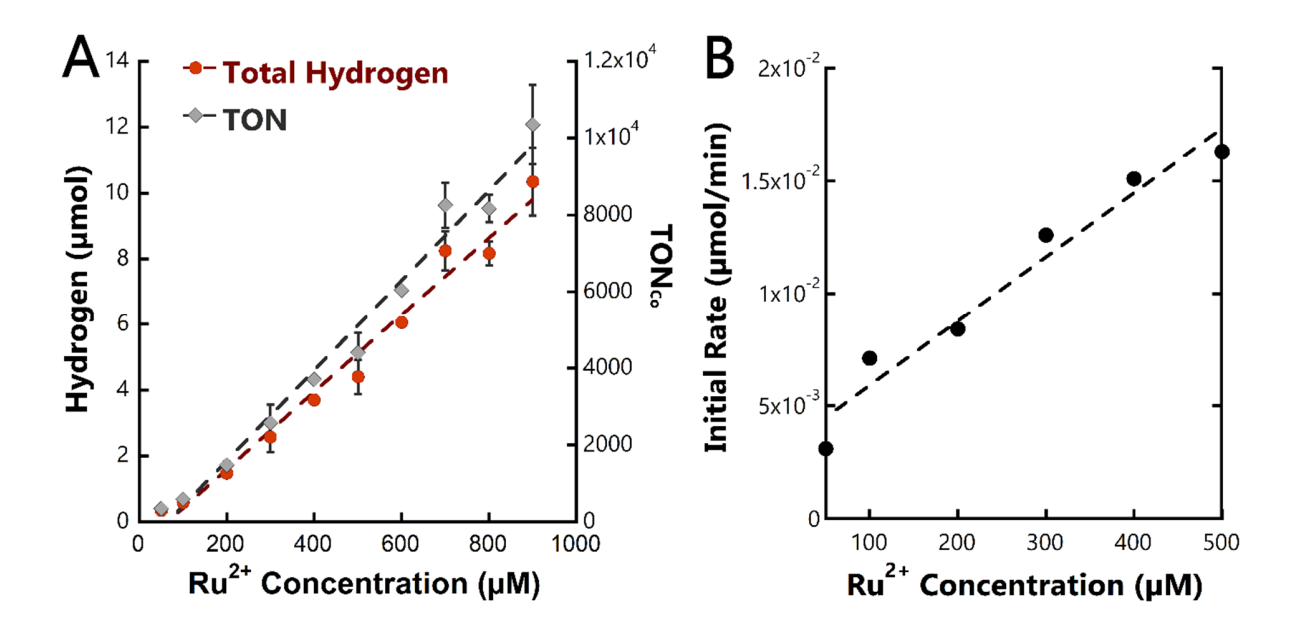


**Fig. 3**. A) Effect of [Ru(bpy)<sub>3</sub>]<sup>2+</sup> concentration (50 - 900 μM) on total H<sub>2</sub> production after 48 hours with 1.0 μM CoMC6\*a and 100 mM ascorbic acid in 1 M piperazine buffer, pH 6.5, sample size 1 mL, with blue (447.5 nm) LED illumination. Error bars represent standard deviation of replicates. B) Initial rates observed with 1.0 μM CoMC6\*a and 100 mM ascorbic acid in 1 M piperazine buffer, pH 6.5, sample size 5 mL, with blue (447.5 nm) LED illumination are linear between 50 μM – 500 μM  $Ru^{2+}$ .

A high (900x molar) excess of photosensitizer yielded the highest TONs in this system, consistent with observations made in similar systems [30, 32, 48, 49]. An increase in H<sub>2</sub> production with photosensitizer concentration is often followed by a decrease or plateau in activity at higher concentrations [30, 49], as observed here. At high concentrations of photosensitizer (> 900 μM), a high optical density likely increases the propensity of dye molecules in a solution to experience both excitation light depletion and self-quenching [77-79]. This may relate to a plateau in H<sub>2</sub> production and decreases in initial rate at high photosensitizer concentrations [34, 41, 49, 50, 73]. Since it seemed that a high excess of sensitizer yielded the greatest amounts of hydrogen, we sought to explore how the sensitizer concentration was impacting the overall stability of the system.

As aforementioned, a limitation of molecular photosensitizers, including  $\mathbf{Ru^{2+}}$ , is degradation across the time of catalysis [74-76, 80]. Pathways to  $\mathbf{Ru^{2+}}$  decomposition have been explored under a variety of conditions [34, 74, 80, 81]. One of the predominant methods of degradation during catalysis is dechelation of a bipyridine ligand [82]. Loss of a bipyridine ligand is accompanied by a loss in the absorption features of the MLCT band ( $\lambda_{max}$  of 452 nm, Fig. 2) of  $\mathbf{Ru^{2+}}$  [61, 82]. Sacrificial electron donor or buffer may take the place of the bipyridine ligand, resulting in a new band that is significantly red shifted [34, 49]. Anticipating that there may be a concentration-dependent effect on  $\mathbf{Ru^{2+}}$  degradation, we observed the UV-vis spectra at a range of concentrations of  $\mathbf{Ru^{2+}}$  post-catalysis.

UV-visible spectra of photocatalysis solutions were measured before and after 48 hours of catalysis with constant concentrations of CoMC6\*a (1  $\mu$ M) and ascorbate (100 mM) and  $Ru^{2+}$  concentrations ranging from 50  $\mu$ M – 900  $\mu$ M. Prior to initiation of photocatalysis, the primary visible bands in each spectrum ( $\lambda_{max} = 452$ ) are attributed to metal-to-ligand charge transfer

(MLCT) transitions from  $\mathbf{Ru^{2+}}$  (Fig S12). The porphyrin Soret band ( $\lambda_{max} = 412$  nm, Fig. 2) is too low in intensity to be observable under these conditions, and ascorbate absorbs strongly toward the UV below 400 nm (Fig. S12). Post-photocatalysis, the appearance of the UV-vis spectra is dependent on Ru<sup>2+</sup> concentration. In solutions containing the lowest Ru<sup>2+</sup> concentration (50 uM – 300 µM), there is a large decrease in intensity at 452 nm, accompanied by the appearance of a broad red-shifted MLCT band (λ<sub>max</sub> of 500 nm, Fig S13). At intermediate concentrations of photosensitizer (400  $\mu$ M – 700  $\mu$ M), there is a decrease in intensity and apparent red shift of the MLCT ( $\lambda_{max}$  of approximately 475 nm), and a shoulder is visible at 500 nm (Fig. S14). At the highest concentrations of sensitizer (800  $\mu$ M – 900  $\mu$ M), the red-shift is the smallest ( $\lambda_{max}$  of approximately 465 nm) and there is not a clear shoulder visible at 500 nm (Fig. S15). Based on these observations, we anticipated that the sensitizer concentration would also impact the longevity of the photocatalytic system. Samples were monitored at time intervals over the course of 48 hours to observe the impact of sensitizer concentration on the longevity of catalysis (Fig. S16). At low sensitizer concentration ( $50 \mu M - 300 \mu M$ ), a plateau in activity is observed within approximately five hours. At intermediate concentrations (400  $\mu$ M - 700  $\mu$ M), activity slows within approximately 25 hours. At the highest excess of sensitizer (greater than 800 µM) activity plateaus after approximately 40 hours.

Appearance of the red-shifted band at 500 nm is correlated to degradation of the sensitizer, as observed elsewhere [49, 50, 82]. Plotting the ratio  $A_{500}$ :  $A_{452}$  nm for each post-photocatalysis sample shows that the degradation observed is linearly dependent on sensitizer concentration (Fig. S17). The diverse dependences on photosensitizer observed across the literature under different experimental conditions [30, 32, 36, 50, 61] imply that while  $\mathbf{Ru^{2+}}$  is chosen to create a model system, the sensitizer may still influence each system in a unique way [80]. The TON, longevity,

and stability of the system described herein is in part limited by the decomposition of the Ru<sup>2+</sup> photosensitizer, particularly in low excess of sensitizer. To overcome the negative impacts of low sensitizer excess, the mimochrome scaffold provides opportunities to tether a sensitizer directly. Residues on the peptide scaffold could be used in a variety of ways, for example a cross-linking reaction between a functionalized sensitizer and a lysine residue in the distal peptide. As other studies have shown, it is possible that directly tethering a sensitizer will improve overall TONs observed in the system [83, 84], although enhancement of unproductive electron transfer is also possible [85]. The development of practical systems incorporating biocatalysts will require an understanding of how both sensitizer and catalyst influence the overall activity of a system.

#### 3.3. Evaluation of cobalt catalysis

Just as the stability of the sensitizer impacts catalysis, the properties of the catalyst influence rate of catalysis, longevity of catalysis, and total hydrogen evolved by the system. To determine the impact of CoMC6\*a on hydrogen evolution catalysis here, the concentration of CoMC6\*a was varied from 0.25  $\mu$ M to 15  $\mu$ M. A constant excess of 100 mM ascorbic acid and 900  $\mu$ M Ru²+, shown above to have the highest total activity in terms of hydrogen evolution, were used to determine total hydrogen produced (Fig. 4). Total hydrogen was gauged after 68 hours, when catalysis has plateaued at high concentrations of sensitizer (Fig. S16). In addition, the dependence of initial rate on catalyst at low concentrations (0 – 4  $\mu$ M) of catalyst was observed. Data was collected approximately every 20 minutes by GC during the first two hours of catalysis (Fig. S18).

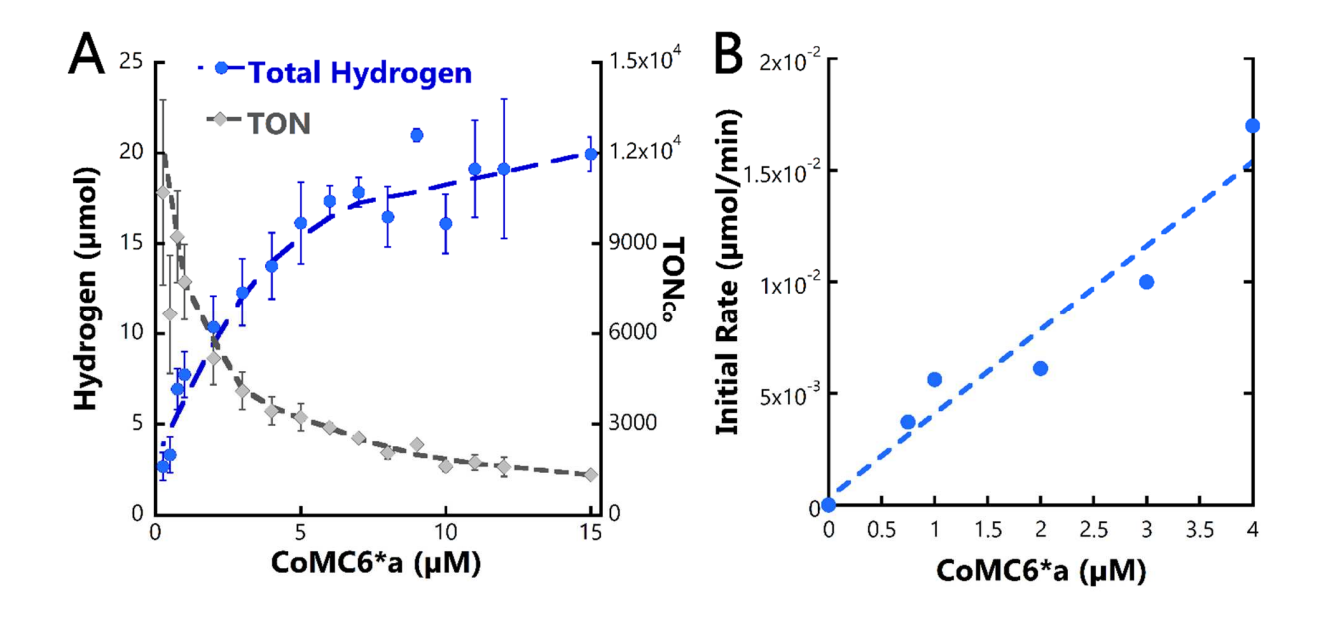


**Fig. 4** A) Effect of CoMC6\*a concentration (0.25 - 15 μM) on total H<sub>2</sub> production with 900 μM Ru<sup>2+</sup> and 100 mM ascorbic acid in 1 M piperazine buffer, pH 6.5, 1 mL sample size, with blue (447.5 nm) LED illumination for 68 hrs. Error bars represent the standard deviation of replicates. B) Initial rates observed with 0 - 4 μM CoMC6\*a, 400 μM **Ru**<sup>2+</sup>, and 100 mM ascorbic acid in 1 M piperazine buffer, pH 6.5, sample volume 5 mL, with blue (447.5 nm) LED illumination.

The amount of  $H_2$  produced increases with increasing concentration of catalyst, beginning to plateau at approximately 5  $\mu$ M catalyst concentration (Fig. 4). The maximum  $H_2$  produced at 15  $\mu$ M CoMC6\*a is 19.9  $\mu$ mol  $\pm$  1.0  $\mu$ mol  $H_2$ , corresponding to a TON of (1.33  $\pm$  0.06) x 10<sup>3</sup>  $\mu$ mol. The minimum  $H_2$  produced at 0.25  $\mu$ M CoMC6\*a is 2.7  $\mu$ mol  $\pm$  0.8  $\mu$ mol, corresponding to the highest TON of (10.7  $\pm$  3.0) x 10<sup>3</sup>  $\mu$ mol. Below the concentration of CoMC6\*a where total hydrogen begins to plateau (0 to 4  $\mu$ M), initial rates of  $H_2$  evolution increase approximately linearly with catalyst concentration (Fig. 3). A maximum initial rate of 1.8 x 10<sup>-2</sup>  $\mu$ mol/min is observed at a catalyst concentration of 4  $\mu$ M (Fig. S18).

Total hydrogen produced begins to plateau at relatively low catalyst concentration (5  $\mu$ M). This observation is consistent with porphyrin catalysts in literature, where plateaus in activity are often observed at micromolar concentrations [30, 32, 48, 50]. Porphyrin catalysts are known to be subject to some aggregation, which can occur at low concentrations [50], but the designed peptide scaffold of CoMC6\*a makes this less likely [51]. As noted earlier, the quenching by the catalyst is extremely efficient, effectively only one order of magnitude less than that by ascorbic acid. As catalyst concentration increases, the effective efficiency of quenching by the catalyst becomes competitive with ascorbic acid, reaching the same order of magnitude by 10  $\mu$ M CoMC6\*a (1.1 x  $10^6$  s<sup>-1</sup> vs 1.8 x  $10^6$  s<sup>-1</sup>). Energy transfer to the catalyst may be one pathway competitive with productive electron transfer from ascorbic acid in the reductive quenching pathway at high catalyst concentration. At low concentrations of catalyst, the linear dependence of rate on catalyst concentration is indicative of a homogenous process. The maximum rates of hydrogen evolution observed here are on the same order of magnitude as our previously introduced biomolecular cobalt catalysts CoGGH (3.6 x  $10^{-2}$   $\mu$ mol/min) [49]and CoMP11-Ac (1.9 x  $10^{-2}$   $\mu$ mol/min) [50].

Cobalt catalysts have been popular for their hydrogen evolution abilities for the past several decades [17, 18, 20, 49]. Some of the best studied are cobalt diglyoxime complexes [27]. The longevity of catalysis observed with CoMC6\*a is higher than for cobalt diglyoxime complexes, known to be unstable [86] in comparable systems [49]. A class of cobalt catalysts built with chelating polypyridyl ligands were developed as one more stable alternative to cobaloximes [35, 87]. Still, CoMC6\*a achieves TONs higher than or on par with the best performing cobalt polypyridyl catalysts, and higher longevity [34, 49, 88]. Cobalt porphyrins have been characterized as promising electrocatalysts for hydrogen evolution [45, 89-91], recently beginning their incorporation in aqueous photochemical systems. Thus far, cobalt porphyrins paired with **Ru**<sup>2+</sup> and

ascorbate include porphyrin [30, 32], porphyrin-peptide [50], and full protein [48, 92] scaffolds (see Fig. S19 for catalyst drawings, Table 1 for catalyst data). As a mini-protein, CoMC6\*a is an interesting intermediate between a functionalized porphyrin and a larger protein. Although several conditions – such as buffer and light intensity – may also impact catalysis, here we make an initial comparison between cobalt porphyrin catalysts paired with **Ru**<sup>2+</sup> and ascorbate (Table 1).

**Table 1.** A comparison of CoMC6\*a to similar cobalt porphyrin catalysts in photochemical systems.<sup>a</sup>

Catalyst	[Cat] (µM)	[Ru <sup>2+</sup> ] (µM)	TON <sub>Co</sub>	TOF (min <sup>-1</sup> )	Longevity <sup>b</sup> (hrs)	pН	Onset Potential (V vs. SHE)
CoTPPS [30]	1.5	1200	6410	120.8	0.7°	6.8	-0.83
CoP [32]	2.5	1000	725	8.8	4 <sup>c</sup>	7	-0.96
CoMyo [48]	1	1000	518	1.47	6°	7	-0.95
Co-cyt <i>b</i> <sub>562</sub> [92]	NR	1000	305	NR	8°	7	-0.95°
CoMP11- Ac [50]	1	350	905	3.2 <sup>d</sup>	20	7.3	-1.0
CoMC6*a	1	900	10400	2.7 <sup>d</sup>	40	6.5	-1.0
	1	400	3700	3.0 <sup>d</sup>	25	6.5	

- a. Table abbreviations: [Cat] is catalyst concentration, [**Ru**<sup>2+</sup>] is sensitizer concentration, TON<sub>Co</sub> is the total turnover number (mole H<sub>2</sub>/mol catalyst), TOF is a turnover frequency (min<sup>-1</sup>), CoTPPS is cobalt *meso*-tetrakis(p-sulfonylphenyl), CoP is cobalt *meso*-tetrakis(1-methylpyridinium-4-yl) porphyrin, CoMyo is cobalt protoporphyrin(IX) substituted into apomyoglobin, Co-cyt is cobalt protoporphyrin(IX) substituted into cytochrome *b*<sub>562</sub> (M7A mutant) and CoMP11-Ac is acetylated cobalt microperoxidase-11
- b. Longevity is estimated from the beginning of the plateau in activity
- c. Estimated from published figure
- d. TOF is a maximum TOF (TON/min) assessed from initial rates of catalysis for comparison to literature examples

One significant metric to compare is the longevity of catalysis. Assessed as time when activity begins to plateau (Table 1), the longevity of catalysis observed is CoMC6\*a > CoMP11-Ac > Co-cyt  $b_{562} \approx$  CoMyo > CoP > CoTPPS. CoMP11-Ac was speculated to be more stable than the protein CoMyo due to the presence of its axial His ligand in a covalently attached peptide [50]. CoMC6\*a also has its axial His in a covalently attached peptide, and additionally has a distal peptide chain scaffolding the porphyrin. The MC6\*a generation of the mimochrome was specifically tailored to boost interaction between the distal chain and the porphyrin [51]. The longevity observed here is consistent with previous trends in an electrochemical study, where CoMC6\*a maintained activity longer than CoMP11-Ac, likely due to additional protection from degradation due to the larger peptide scaffold [53]. In addition, CoMC6\*a is stable under irradiation, with few changes in the Soret band observed over 48 hours of irradiation (Fig. S20). At low concentration of sensitizer, which facilitates observation of the Soret band, the MLCT band of Ru<sup>2+</sup> degrades while the Soret band remains consistent (Fig. S21). As catalyst concentration was varied, the degradation of Ru<sup>2+</sup> was observed by UV-vis (Fig. S22). Unlike when varying concentrations of Ru<sup>2+</sup>, the degradation does not appear to depend on catalyst concentration in high excess of Ru<sup>2+</sup> (Fig. S23). Consequently, the stability of the system seems to be limited by the concentration of  $\mathbf{R}\mathbf{u}^{2+}$  more than the concentration of catalyst.

Turnover numbers (TONs) and frequencies (TOFs) both reflect system activity; TON reflects longevity as well. TONs observed under conditions herein for CoMC6\*a are higher than the other cobalt porphyrins, notably outperforming CoMP11-Ac and CoMyo by 10x under optimized conditions (Table 1). The maximum rates (initial rates, shown as TOFs) observed for CoMC6\*a are on the same order of magnitude as those for both CoMP11-Ac and CoMyo. At similar concentrations of photosensitizer, CoMC6\*a evolves hydrogen slightly faster than CoMyo (2.7 min<sup>-1</sup> vs. 1.45 min<sup>-1</sup>), but slightly slower than CoMP11-Ac and CoP (3.2 min<sup>-1</sup> vs. 8.8 min<sup>-1</sup>) and significantly slower than CoTPPS (120.8 min<sup>-1</sup>). Uniquely from the other cobalt porphyrins described here, CoMyo and CoMC6\*a both have distal peptide chains sandwiching the porphyrin, which may impact catalysis. The pockets of both CoMC6\*a and CoMyo are somewhat hydrophobic in nature – in the case of CoMC6\*a, this can be altered by design [51]. The presence of the distal peptide may impact proton transfer reactions [93], and it may also present opportunities for new reactivity. For example, in electrocatalysis, hydrophobicity has helped to favor CO<sub>2</sub> reduction over proton reduction [94]. Recently, incorporation of cobalt protoporphyrin IX into cytochrome  $b_{562}$ , which has a hydrophobic pocket, demonstrated that the protein scaffold promoted CO<sub>2</sub> reduction [95]. Conversely, incorporating residues to aid proton transfer into the pocket increased hydrogen evolution activity [92]. The proton transfer reactions of CoMC6\*a will likely be more amenable to tuning than for a catalyst like CoMP11-Ac, and may present opportunities for new reactivity like CO<sub>2</sub> reduction.

#### 3.4 Effects of pH

An attractive feature of the photocatalytic systems featuring cobalt porphyrin catalysts is their ability to function near neutral pH (Table 1). Furthermore, their optimal activity tends to occur near pH 7. This contrasts with many other water-soluble cobalt catalysts, including cobalt

glyoximes and cobalt polypyridyls, which tend to produce the most hydrogen at an acidic pH (approximately pH 4 – 6) [14, 17, 20, 34-37, 41, 60, 61]. We sought to determine if CoMC6\*a would behave similarly to other cobalt porphyrins by varying pH and monitoring total hydrogen evolution. The pH was varied from 2.5 to 10.5, and hydrogen evolution was measured after 48 hours. CoMC6\*a is stable across this range, as evidenced by its absorbance spectrum (Fig. S24). The highest hydrogen evolution was observed at a pH of 7, peaking at 5.79  $\mu$ mol  $\pm$  0.20  $\mu$ mol H<sub>2</sub>. The lowest amount of hydrogen evolved was at pH 2.5, where activity was almost completely suppressed and only 0.38  $\mu$ mol  $\pm$  0.01  $\mu$ mol H<sub>2</sub> were produced. Some activity was sustained even at highly basic pH, with the system producing 2.09  $\mu$ mol  $\pm$  0.45  $\mu$ mol H<sub>2</sub> at pH 10.5. Initial rates during the first three hours of catalysis (Fig. S25) mirror this trend, peaking at pH 7.2 (3.0 x 10<sup>-2</sup>  $\mu$ mol/min), and decreasing at acidic and basic pH (Fig. 5).

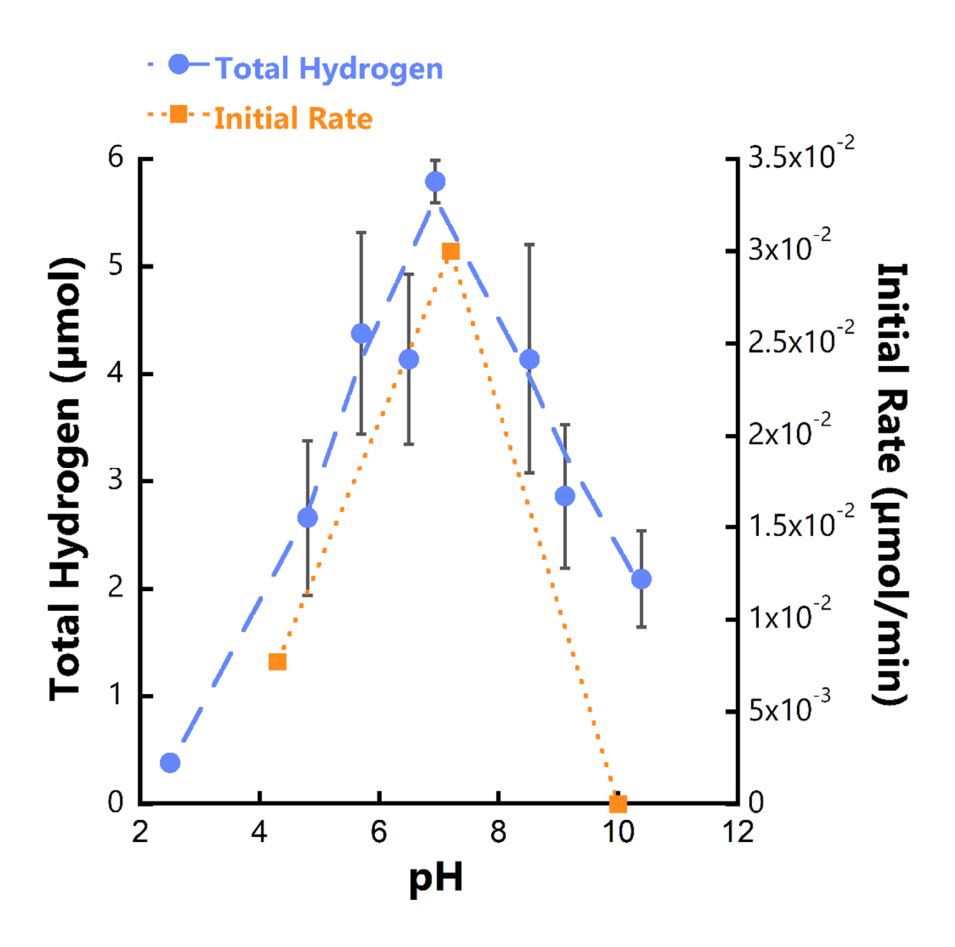


**Fig. 5.** Effect of pH on  $H_2$  production with 400  $\mu$ M  $Ru^{2+}$ , 1  $\mu$ M CoMC6\*a, and 100 mM ascorbic acid in 1 M piperazine buffer, pH ranging from 2.5 – 10.5 (shown), 1 mL sample size, with blue (447.5 nm) LED illumination for 48 hrs. Error bars represent standard deviations of replicates.

The cobalt catalysts referenced herein – cobalt porphyrins, cobalt glyoximes, and cobalt polypyridyls – have been paired with  $\mathbf{Ru^{2+}}$  and ascorbate. Yet, as aforementioned, a particular pH preference is shown depending on the catalyst. The speciation of ascorbate has been implicated in the decreases in activity at low pH. Since ascorbate is the primary electron donor, protonation to ascorbic acid (pK<sub>a</sub> 4.1) decreases the efficiency of the quencher, as observed previously [50, 60]. Consistent with this observation, the hydrogen evolution activity decreases substantially below a

pH of 4.5 here. While this effect on electron donor accounts for decreases in activity at acidic pH, it does not account for the discrepancies in pH preference of cobalt catalysts (acidic vs. neutral), or decreases in total hydrogen at basic pH values.

The synthetic catalyst Co(dmgH)<sub>2</sub>(py)Cl (dmgH =dimethylglyoxime, py =pyridine) was recently used to probe pH-dependent effects at work in a similar photochemical system [60]. There are multiple protonation steps necessary at a catalytic cobalt catalyst for hydrogen evolution to occur (Fig. S26). The key reason for decreases at high pH in the work on Co(dmgH)<sub>2</sub>(py)Cl was hypothesized to be inhibition of protonation of Co(I) to Co(III)-H, with a calculated pK<sub>a</sub> of 7.7. As pH increased beyond 7, protonation was not favored, stalling proton reduction activity. In our recent work characterizing photochemical hydrogen evolution using CoMP11-Ac, we highlighted that the decreases in activity at basic pH may reflect disfavoring a protonation step, decelerating catalysis. Here, at basic pH (pH 10), no detectable hydrogen is produced from CoMC6\*a within the first three hours of catalysis, although longer experiments do yield detectable hydrogen (Fig. S25, Fig. 5). This decrease in activity at high pH is consistent with a protonation step impacting catalysis being slowed at basic pH. In comparison to CoMP11-Ac, CoMC6\*a is similar in that maximum activity is achieved within ± 0.5 pH units of pH 7. Unlike CoMP11-Ac, though, CoMC6\*a remains active at basic pH (8.5 – 10.5). At a pH of 9.1, CoMC6\*a achieves a TON of 2,860. Conversely, at pH 9.5, CoMP11 yielded a TON of 150 [50]. Likely aiding the total activity of CoMC6\*a at basic pH is the longevity of catalysis, which is higher for CoMC6\*a than CoMP11-Ac. In mechanistic work on the proton reduction of CoMC6\*a in water, the pKa for protonation of a Co(I) species to a Co(III)-H was speculated to be high (potentially ~8.7) [54]. If indeed CoMC6\*a has a higher pKa for a key protonation event than estimated for a typical cobalt porphyrin [89], that would be consistent with an increase in sustained activity at basic pH values.

CoMC6\*a presents a unique opportunity to probe the impact of biocatalyst structure on catalytic activity in a photochemical system in water. Unlike CoMP11-Ac, the mimochrome scaffold is easily tailorable [51]. For example, is possible to change the axial ligation to a ligand other than histidine, which can influence electron density at the metal and proton transfers to the metal site. Moving forward, the scaffold of CoMC6\*a will be altered to gain more detailed mechanistic information about proton reduction in the photochemical system.

#### 4. Conclusion

CoMC6\*a, a cobalt derivative of mimochromes, is a synthetic mini-protein shown to act as a hydrogenase functional mimic in a photochemical system. While CoMC6\*a maintains the benefits of previously introduced biomolecular catalysts – namely water solubility and robust activity - it also introduces new advantages. Relative to other water-soluble cobalt porphyrin systems, particularly the related cobalt porphyrin-peptide CoMP11-Ac, CoMC6\*a demonstrates higher longevity and activity. Active for up to 40 hours and yielding TONs over 10,000, CoMC6\*a is not only highly active, but it also creates a space for unique opportunities moving forward. The high stability of CoMC6\*a may be heightened even further by immobilization in a solar fuel production system [96]. The recent achievement of a nonnative de novo synthesis of cobalt porphyrins in E. coli shows great promise for the development of cobalt porphyrin containing proteins [97]. The highly tunable nature of the mimochrome scaffold provides a path for deepening our understanding of how designed protein structure impacts proton reduction activity. The ability to tune overpotential of catalysis via protein folding may permit the use of less-reducing, nonmetal containing photosensitizers. The ability to tailor the active site of CoMC6\*a may promote new reactivity altogether, broadening the growing arsenal of biomolecular catalysts for solar-tofuel chemistry.

#### 5. Acknowledgement

The authors are grateful to Prof. Vincenzo Pavone for his early mimochrome design.

This work is supported by the U.S. Department of Energy, Office of Science, Office of Basic Energy Sciences [Award DE-FG02-09ER16121]. E.H.E. acknowledges support by the National Institutes of Health Training Grant in the Chemistry-Biology Interface [T32-GM118283]. A.A.S. acknowledges support from the National Science Foundation Graduate Research Fellowship Program [DGE-1939268]. This material is based upon work supported by the National Science Foundation Graduate Research Fellowship Program. Any opinions, findings, and conclusions or recommendations expressed in this material are those of the author(s) and do not necessarily reflect the views of the National Science Foundation.

#### **References**

- [1] S. Zhu, D. Wang, Photocatalysis: Basic Principles, Diverse Forms of Implementations and Emerging Scientific Opportunities, *Adv. Energy. Mater.*, 7 (2017) 1700841. doi: 10.1002/aenm.201700841
- [2] Q. Liu, L.-Z. Wu, Recent advances in visible-light-driven organic reactions, *Natl. Sci. Rev.* 4 (2017) 359-380. doi: 10.1093/nsr/nwx039
- [3] E.H. Edwards, K.L. Bren, Light-driven catalysis with engineered enzymes and biomimetic systems, *Biotechnol. Appl. Biochem.* 67 (2020) 463-483. doi:10.1002/bab.1976
- [4] G. Chen, G.I.N. Waterhouse, R. Shi, J. Zhao, Z. Li, L.-Z. Wu, C.-H. Tung, T. Zhang, From Solar Energy to Fuels: Recent Advances in Light-Driven C1 Chemistry, *Angew. Chem. Int. Ed.* 58 (2019) 17528-17551. doi: 10.1002/anie.201814313
- [5] J. Su, L. Vayssieres, A Place in the Sun for Artificial Photosynthesis? *ACS Energy Lett.* 1 (2016) 121-135. doi: 10.1021/acsenergylett.6b00059
- [6] G. Ciamician, The Photochemistry of the Future, *Science* 36 (1912) 385-394. doi:10.1126/science.36.926.385
- [7] A.J. Bard, M.A. Fox, Artificial Photosynthesis: Solar Splitting of Water to Hydrogen and Oxygen. *Acc. Chem. Res.* 28 (1995) 141-145. doi:10.1021/ar00051a007
- [8] Y. Wang, A. Vogel, M. Sachs, R.S. Sprick, L. Wilbraham, S.J.A. Moniz, R. Godin, M.A. Zwijnenburg, J.R. Durrant, A.I. Cooper, J. Tang, Current understanding and challenges of solar-driven hydrogen generation using polymeric photocatalysts, *Nat. Energy* 4 (2019) 746-760. doi: 10.1038/s41560-020-0651-4
- [9] B. Zhang, L. Sun, Artificial photosynthesis: opportunities and challenges of molecular catalysts, *Chem. Soc. Rev.* 48 (2019) 2216-2264. doi:10.1039/C8CS00897C

- [10] I.P. Jain, Hydrogen the fuel for 21st century, *Int. J. Hydrogen Energy* 34 (2009) 7368-7378. doi: 10.1016/j.ijhydene.2009.05.093
- [11] J.W. Tye, M.B. Hall, M.Y. Darensbourg, Better than platinum? Fuel cells energized by enzymes, *PNAS* 102 (2005) 16911-16912. doi: 10.1073/pnas.0508740102
- [12] P.-P. Liebgott, A.L. de Lacey, B. Burlat, L. Cournac, P. Richaud, M. Brugna, V.M. Fernandez, B. Guigliarelli, M. Rousset, C. Léger, S. Dementin, Original Design of an Oxygen-Tolerant [NiFe] Hydrogenase: Major Effect of a Valine-to-Cysteine Mutation near the Active Site, *J. Am. Chem. Soc.* 133 (2011) 986-997. doi: 10.1021/ja108787s
- [13] A. Abou Hamdan, S. Dementin, P.-P. Liebgott, O. Gutierrez-Sanz, P. Richaud, A.L. De Lacey, M. Rousset, P. Bertrand, L. Cournac, C. Léger, Inhibition and Aerobic Inactivation Kinetics of Desulfovibrio fructosovorans NiFe Hydrogenase Studied by Protein Film Voltammetry, *J. Am. Chem. Soc.* 134, (2012) 8368-8371. doi: 10.1021/ja046548d [14] P. Du, R. Eisenberg, Catalysts made of earth-abundant elements (Co, Ni, Fe) for water splitting: Recent progress and future challenges, *Energy Environ. Sci.* 5 (2012) 6012-6021.
- [15] J.R. McKone, S.C. Marinescu, B.S. Brunschwig, J.R. Winkler, H.B. Gray, Earth-abundant hydrogen evolution electrocatalysts, *Chem. Sci.* 5 (2014) 865-878. doi: doi.org/10.1039/C3SC51711J

doi:10.1039/C2EE03250C

[16] M.A. Gross, A. Reynal, J.R. Durrant, E. Reisner, Versatile Photocatalytic Systems for H<sub>2</sub> Generation in Water Based on an Efficient DuBois-Type Nickel Catalyst, *J. Am. Chem. Soc.* 136 (2014) 356-366. doi: doi.org/10.1021/ja410592d

- [17] W.T. Eckenhoff, Molecular catalysts of Co, Ni, Fe, and Mo for hydrogen generation in artificial photosynthetic systems, *Coord. Chem. Rev.* 373 (2018) 295-316. doi:10.1016/j.ccr.2017.11.002
- [18] W.T. Eckenhoff, W.R. McNamara, P. Du, R. Eisenberg, Cobalt complexes as artificial hydrogenases for the reductive side of water splitting, *Biochim. Biophys. Acta, Bioenerg.* 1827 (2013) 958-973. doi:10.1016/j.bbabio.2013.05.003
- [19] L. Kohler, J. Niklas, R.C. Johnson, M. Zeller, O.G. Poluektov, K.L. Mulfort, Molecular Cobalt Catalysts for H<sub>2</sub> Generation with Redox Activity and Proton Relays in the Second Coordination Sphere, *Inorg. Chem.* 58 (2019) 1697-1709. doi:10.1021/acs.inorgchem.8b03297 [20] V. Artero, M. Chavarot-Kerlidou, M. Fontecave, Splitting Water with Cobalt, *Angew. Chem. Int. Ed.* 50 (2011) 7238-7266. doi: 10.1002/anie.201007987
- [21] P.-A. Jacques, V. Artero, J. Pécaut, M. Fontecave, Cobalt and nickel diimine-dioxime complexes as molecular electrocatalysts for hydrogen evolution with low overvoltages, *PNAS* 106 (2009) 20627-20632.
- [22] P. Du, J. Schneider, G. Luo, W.W. Brennessel, R. Eisenberg, Visible Light-Driven Hydrogen Production from Aqueous Protons Catalyzed by Molecular Cobaloxime Catalysts, *Inorg. Chem.* 48 (2009) 4952-4962. doi:10.1021/ic900389z
- [23] D.W. Wakerley, E. Reisner, Development and understanding of cobaloxime activity through electrochemical molecular catalyst screening, *Phys. Chem. Chem. Phys.* 16 (2014) 5739-5746. doi:10.1039/C4CP00453A
- [24] J.L. Dempsey, B.S. Brunschwig, J.R. Winkler, H.B. Gray, Hydrogen Evolution Catalyzed by Cobaloximes, *Acc. Chem. Res.* 42 (2009) 1995-2004. doi:10.1021/ar900253e

- [25] A. Panagiotopoulos, K. Ladomenou, D. Sun, V. Artero, A.G. Coutsolelos, Photochemical hydrogen production and cobaloximes: the influence of the cobalt axial N-ligand on the system stability, *Dalton Trans.*,45 (2016) 6732-6738. doi: 10.1039/C5DT04502A
- [26] M. Bacchi, G. Berggren, J. Niklas, E. Veinberg, M.W. Mara, M.L. Shelby, O.G. Poluektov, L.X. Chen, D.M. Tiede, C. Cavazza, M.J. Field, M. Fontecave, V. Artero, Cobaloxime-Based Artificial Hydrogenases, *Inorg. Chem.* 53 (2014) 8071-8082. doi:10.1021/ic501014c
- [27] B.H. Solis, S. Hammes-Schiffer, Substituent Effects on Cobalt Diglyoxime Catalysts for Hydrogen Evolution, *J. Am. Chem. Soc.* 133 (2011) 19036-19039. doi:
- [28] W.R. McNamara, Z. Han, P.J. Alperin, W.W. Brennessel, P.L. Holland, R. Eisenberg, A Cobalt–Dithiolene Complex for the Photocatalytic and Electrocatalytic Reduction of Protons. *J. Am. Chem. Soc.* 133 (2011) 15368-15371. doi:10.1021/ja207842r
- [29] W.R. McNamara, Z. Han, C.-J. Yin, W.W. Brennessel, P.L. Holland, R. Eisenberg, Cobalt-dithiolene complexes for the photocatalytic and electrocatalytic reduction of protons in aqueous solutions, *PNAS* 109 (2012) 15594-15599. doi: 10.1073/pnas.1120757109
- [30] B.B. Beyene, C-H. Hung, Photocatalytic hydrogen evolution from neutral aqueous solution by a water-soluble cobalt(II) porphyrin, *Sustain. Energy Fuels* 2 (2018) 2036-2043. doi:10.1039/C8SE00253C
- [31] W. Zhang, W. Lai, R. Cao, Energy-Related Small Molecule Activation Reactions: Oxygen Reduction and Hydrogen and Oxygen Evolution Reactions Catalyzed by Porphyrin- and Corrole-Based Systems, *Chem. Rev.* 117 (2017) 3717-3797. doi:10.1021/acs.chemrev.6b00299
  [32] M. Natali, A. Luisa, E. Iengo, F. Scandola, Efficient photocatalytic hydrogen generation from water by a cationic cobalt(II) porphyrin, *Chem. Comm.* 50 (2014) 1842-1844. doi:10.1039/C3CC48882A

- [33] M.M. Roubelakis, D.K. Bediako, D.K. Dogutan, D.G. Nocera, Proton-coupled electron transfer kinetics for the hydrogen evolution reaction of hangman porphyrins. *Energy Environ*. *Sci.* 5 (2012) 7737-7740. doi: 10.1039/C2EE21123H
- [34] R.S. Khnayzer, V.S. Thoi, M. Nippe, A.E. King, J.W. Jurss, K.A. El Roz, J.R. Long, C.J. Chang, F.N. Castellano, Towards a comprehensive understanding of visible-light photogeneration of hydrogen from water using cobalt(II) polypyridyl catalysts, *Energy Environ*. *Sci.* 7 (2014) 1477-1488. doi:10.1039/C3EE43982H
- [35] N. Queyriaux, R.T. Jane, J. Massin, V. Artero, M. Chavarot-Kerlidou, Recent developments in hydrogen evolving molecular cobalt(II)–polypyridyl catalysts, *Coord. Chem. Rev.* 304 (2015) 3-19. doi:10.1016/j.ccr.2015.03.014
- [36] M. Natali, E. Badetti, E. Deponti, M. Gamberoni, F.A. Scaramuzzo, A. Sartorel, C. Zonta, Photoinduced hydrogen evolution with new tetradentate cobalt(II) complexes based on the TPMA ligand, *Dalton Trans.* 45 (2016) 14764-14773. doi:10.1039/C6DT01705C
- [37] E. Deponti, A. Luisa, M. Natali, E. Iengo, F. Scandola, Photoinduced hydrogen evolution by a pentapyridine cobalt complex: elucidating some mechanistic aspects, *Dalton Trans.*, 43 (2014) 16345-16353. doi:10.1039/C4DT02269F
- [38] C. Bachmann, M. Guttentag, B. Spingler, R. Alberto, A Highly Stable Rhenium–Cobalt System for Photocatalytic H<sub>2</sub> Production: Unraveling the Performance-Limiting Steps, *Inorg. Chem.* 52 (2013) 6055-6061. doi: 10.1021/ic100036v
- [39] M. Vennampalli, G. Liang, L. Katta, C.E. Webster, X. Zhao, Electronic Effects on a Mononuclear Co Complex with a Pentadentate Ligand for Catalytic H<sub>2</sub> Evolution, *Inorg. Chem.* 53 (2014) 10094-10100. doi:10.1021/ic500840e

- [40] A. Rodenberg, M. Orazietti, B. Probst, C. Bachmann, R. Alberto, K.K. Baldridge, P. Hamm, Synthesis, Characterization, and Photocatalytic H<sub>2</sub>-Evolving Activity of a Family of [Co(N4Py)(X)]<sup>n+</sup> Complexes in Aqueous Solution, *Inorg. Chem.* 54 (2015) 646-657. doi: 10.1021/acs.inorgchem.6b00391
- [41] M. Nippe, R.S. Khnayzer, J.A. Panetier, D.Z. Zee, B.S. Olaiya, M. Head-Gordon, C.J. Chang, F.N. Castellano, J.R. Long, Catalytic protonreduction with transition metal complexes of the redox-active ligand bpy2PYMe, *Chem. Sci.* 4 (2013) 3934-3945. doi: 10.1039/C3SC51660A [42] S. Berardi, S. Drouet, L. Francàs, C. Gimbert-Suriñach, M. Guttentag, C. Richmond, T. Stoll, A. Llobet, Molecular artificial photosynthesis, *Chem. Soc. Rev.* 43 (2014) 7501-7519. doi:10.1039/C3CS60405E
- [43] W. Lubitz, H. Ogata, O. Rüdiger, E. Reijerse, Hydrogenases, *Chem. Rev.* 114 (2014) 4081-4148. doi:10.1021/cr4005814
- [44] P.D. Tran, J. Barber, Proton reduction to hydrogen in biological and chemical systems, *Phys. Chem. Chem. Phys.* 14 (2012) 13772-13784. doi: 10.1039/C2CP42413D
- [45] J.M. Le, K.L. Bren, Engineered Enzymes and Bioinspired Catalysts for Energy Conversion, *ACS Energy Lett.* 4 (2019) 2168-2180. doi: 10.1021/acsenergylett.9b01308
- [46] M. Bacchi, E. Veinberg, M.J. Field, J. Niklas, T. Matsui, D.M. Tiede, O.G. Poluektov, M. Ikeda-Saito, M. Fontecave, V. Artero, Artificial Hydrogenases Based on Cobaloximes and Heme Oxygenase, *ChemPlusChem* 81 (2016) 1083-1089. doi:10.1002/cplu.201600218
- [47] S.R. Soltau, J. Niklas, P.D. Dahlberg, O.G. Poluektov, D.M. Tiede, K.L. Mulfort, L.M. Utschig, Aqueous light driven hydrogen production by a Ru–ferredoxin–Co biohybrid, *Chem. Comm.* 51 (2015) 10628-10631. doi:10.1039/C5CC03006D

- [48] D.J. Sommer, M.D. Vaughn, G. Ghirlanda, Protein secondary-shell interactions enhance the photoinduced hydrogen production of cobalt protoporphyrin IX, *Chem. Comm.* 50 (2014) 15852-15855. doi:10.1039/C4CC06700B
- [49] S. Chakraborty, E.H. Edwards, B. Kandemir, K.L. Bren, Photochemical Hydrogen Evolution from Neutral Water with a Cobalt Metallopeptide Catalyst, *Inorg. Chem.* 58 (2019) 16402-16410. doi:10.1021/acs.inorgchem.9b02067
- [50] E.H. Edwards, J. Jelušić, S. Chakraborty, K.L. Bren, Photochemical hydrogen evolution from cobalt microperoxidase-11, *J. Inorg. Biochem.* 217 (2021) 111384. doi: 10.1016/j.jinorgbio.2021.111384
- [51] L. Leone, M. Chino, F. Nastri, O. Maglio, V. Pavone, A. Lombardi, Mimochrome, a metalloporphyrin-based catalytic Swiss knife, *Biotechnol. Appl. Biochem.* 67 (2020) 495-515. doi: 10.1002/bab.1985
- [52] L. Leone, D. D'Alonzo, O. Maglio, V. Pavone, F. Nastri, A. Lombardi, Highly Selective Indole Oxidation Catalyzed by a Mn-Containing Artificial Mini-Enzyme, *ACS Catal.* 11 (2021) 9407-9417. doi: 10.1021/acscatal.1c01985
- [53] V. Firpo, J.M. Le, V. Pavone, A. Lombardi, K.L. Bren, Hydrogen evolution from water catalyzed by cobalt-mimochrome VI\*a, a synthetic mini-protein, *Chem. Sci.* 9 (2018) 8582-8589. doi:10.1039/C8SC01948G
- [54] J.M. Le, G. Alachouzos, M. Chino, A.J. Frontier, A. Lombardi, K.L. Bren, Tuning Mechanism through Buffer Dependence of Hydrogen Evolution Catalyzed by a Cobalt Minienzyme, *Biochemistry* 59 (2020) 1289-1297. doi: 10.1021/acs.biochem.0c00060
- [55] G. Caserta, M. Chino, V. Firpo, G. Zambrano, L. Leone, D. D'Alonzo, F. Nastri, O. Maglio,
   V. Pavone, A. Lombardi, *ChemBioChem*, 19, (2018) 1823-1826. doi: 10.1002/cbic.201800200

- [56] K. Kalyanasundaram, Photophysics, photochemistry and solar energy conversion with tris(bipyridyl)ruthenium(II) and its analogues, *Coord. Chem. Rev.* 46 (1982) 159-244. doi:10.1016/0010-8545(82)85003-0
- [57] W.T. Eckenhoff, R. Eisenberg, Molecular systems for light driven hydrogen production, *Dalton Trans.* 41 (2012) 13004-13021. doi:10.1039/C2DT30823A
- [58] A. Mazzeo, S. Santalla, C. Gaviglio, F. Doctorovich, J. Pellegrino, Recent progress in homogeneous light-driven hydrogen evolution using first-row transition metal catalysts, *Inorg. Chim. Acta* 517 (2021) 119950. doi: 10.1016/j.ica.2020.119950
- [59] C.V. Krishnan, N. Sutin, Homogeneous catalysis of the photoreduction of water by visible light. 2. Mediation by a tris(2,2'-bipyridine)ruthenium(II)-cobalt(II) bipyridine system, *J. Am. Chem. Soc.* 103 (1981) 2141-2142. doi:10.1021/ja00398a066
- [60] M. Natali, Elucidating the Key Role of pH on Light-Driven Hydrogen Evolution by a Molecular Cobalt Catalyst, *ACS Catal.* 7 (2017) 1330-1339. doi:10.1021/acscatal.6b03087 [61] E. Deponti, M. Natali, Photocatalytic hydrogen evolution with ruthenium polypyridine sensitizers: unveiling the key factors to improve efficiencies, *Dalton Trans.* 45 (2016) 9136-9147. doi:10.1039/C6DT01221C
- [62] Y. Pellegrin, F. Odobel, Sacrificial electron donor reagents for solar fuel production. *C. R. Chim.* 20 (2017) 283-295. doi:10.1016/j.crci.2015.11.026
- [63] C.R. Bock, J.A. Connor, A.R. Gutierrez, T.J. Meyer, D.G. Whitten, B.P. Sullivan, J.K. Nagle, Estimation of excited-state redox potentials by electron-transfer quenching. Application of electron-transfer theory to excited-state redox processes, *J. Am. Chem. Soc.* 101 (1979) 4815-4824. doi:10.1021/ja00511a007

- [64] C. Creutz, Complexities of ascorbate as a reducing agent, *Inorg. Chem.* 20 (1981) 4449-4452. doi:10.1021/ic50226a088
- [65] C. Esmieu, P. Raleiras, G. Berggren, From protein engineering to artificial enzymes biological and biomimetic approaches towards sustainable hydrogen production, *Sustain. Energy Fuels* 2 (2018) 724-750. doi:10.1039/C7SE00582B
- [66] H. Liu, L. Wei, F. Liu, Z. Pei, J. Shi, Z.-j. Wang, D. He, Y. Chen, Homogeneous, Heterogeneous, and Biological Catalysts for Electrochemical N<sub>2</sub> Reduction toward NH<sub>3</sub> under Ambient Conditions, *ACS Catal.*, 9 (2019) 5245-5267. doi: 10.1021/acscatal.9b00994

  [67] D. Kishore Kumar, J. Kříž, N. Bennett, B. Chen, H. Upadhayaya, K.R. Reddy, V. Sadhu, Functionalized metal oxide nanoparticles for efficient dye-sensitized solar cells (DSSCs): A review, Mater. Sci. for Energy Technol., 3 (2020) 472-481. doi: 10.1016/j.mset.2020.03.003

  [68] S. Garakyaraghi, F.N. Castellano, Nanocrystals for Triplet Sensitization: Molecular Behavior from Quantum-Confined Materials, *Inorg. Chem.*, 57 (2018) 2351-2359. doi: 10.1021/acs.inorgchem.7b03219
- [69] J. Jasieniak, M. Califano, S.E. Watkins, Size-Dependent Valence and Conduction Band-Edge Energies of Semiconductor Nanocrystals, *ACS Nano* 5 (2011) 5888-5902. doi: 10.1021/nn201681s
- [70] C. Mongin, S. Garakyaraghi, N. Razgoniaeva, M. Zamkov, F.N. Castellano, Direct observatio of triplet energy transfer from semiconductor nanocrystals, *Science*, 351 (2016) 369-372. doi: 10.1126/science.aad6378
- [71] J. Zhao, W. Wu, J. Sun, S. Guo, Chemical Society Reviews, Triplet photosensitizers: from moleclar design to applications, *Chem. Soc. Rev.* 42 (2013) 5323-5351.

doi:10.1039/C3CS35531D

- [72] X. Zhao, Y. Hou, L. Liu, J. Zhao, Triplet Photosensitizers Showing Strong Absorption of Visible Light and Long-Lived Triplet Excited States and Application in Photocatalysis: A Mini Review, *Energy Fuels*, (2021). doi: 10.1021/acs.energyfuels.1c02130
- [73] J.I. Goldsmith, W.R. Hudson, M.S. Lowry, T.H. Anderson, S. Bernhard, Discovery and High-Throughput Screening of Heteroleptic Iridium Complexes for Photoinduced Hydrogen Production, J. Am. Chem. Soc. 127 (2005) 7502-7510. doi:10.1021/ja0427101
- [74] B. Limburg, E. Bouwman, S. Bonnet, Rate and Stability of Photocatalytic Water Oxidation using [Ru(bpy)3]2+ as Photosensitizer, *ACS Catal.* 6 (2016) 5273-5284. doi: 10.1021/acscatal.6b00107
- [75] P.K. Ghosh, B.S. Brunschwig, M. Chou, C. Creutz, N. Sutin, Thermal and light-induced reduction of the ruthenium complex cation Ru(bpy)<sub>3</sub><sup>3+</sup> in aqueous solution, J. Am. Chem. Soc 106 (1984) 4772-4783. doi: 10.1021/ja00329a022
- [76] M. Hara, C.C. Waraksa, J.T. Lean, B.A. Lewis, T.E. Mallouk, Photocatalytic Water Oxidation in a Buffered Tris(2,2'-bipyridyl)ruthenium Complex-Colloidal IrO<sub>2</sub> System, *J. Phys. Chem A* 104 (2000) 5275-5280. doi: 10.1021/jp000321x
- [77] W. Bae, T.-Y. Yoon, C. Jeong, Direct evaluation of self-quenching behavior of fluorophores at high concentrations using an evanescent field, *PLoS ONE*, 16 (2021) e0247326. doi: 10.1371/journal.pone.0247326
- [78] E.M. Gholizadeh, L. Frazer, R.W. MacQueen, J.K. Gallaher, T.W. Schmidt, Photochemical upconversion is suppressed by high concentrations of molecular sensitizers, *Phys. Chem. Chem. Phys.* 20 (2018) 19500-19506. doi: 0.1039/C8CP02650E
- [79] J.R. Lakowicz, Principles of fluorescence spectroscopy, Springer, New York, (2006). doi: 10.1007/978-0-387-46312-4

- [80] U.S. Akhtar, E.L. Tae, Y.S. Chun, I.C. Hwang, K.B. Yoon, Insights into Decomposition Pathways and Fate of Ru(bpy)<sub>3</sub><sup>2+</sup> during Photocatalytic Water Oxidation with S<sub>2</sub>O<sub>8</sub><sup>2-</sup> as Sacrificial Electron Acceptor, *ACS Catal.* 6 (2016) 8361-8369. doi: 10.1021/acscatal.6b02595 [81] A. Vaidyalingam, P.K. Dutta, Analysis of the Photodecomposition Products of Ru(bpy)<sub>3</sub><sup>2+</sup> in Various Buffers and upon Zeolite Encapsulation, Anal. Chem. 72 (2000) 5219-5224. doi:10.1021/ac000408e
- [82] A. Soupart, F. Alary, J-L. Heully, P.I.P. Elliott, I.M. Dixon, Theoretical Study of the Full Photosolvolysis Mechanism of [Ru(bpy)<sub>3</sub>]<sup>2+</sup>: Providing a General Mechanistic Roadmap for the Photochemistry of [Ru(N^N)<sub>3</sub>]<sup>2+</sup>-Type Complexes toward Both Cis and Trans Photoproducts, *Inorg. Chem.* 59 (2020) 14679-14695. doi:10.1021/acs.inorgchem.0c01843
- [83] A. Jacques, O. Schott, K. Robeyns, G.S. Hanan, B. Elias, Hydrogen Photoevolution from a Green-Absorbing Iridium(III)-Cobalt(III) Dyad, *Eur. J. Inorg. Chem.*, 12 (2016) 1779-1783. doi: 10.1002/ejic.201501467
- [84] C. Lentz, O. Schott, T. Auvray, G. Hanan, B. Elias, Photocatalytic Hydrogen Production Using a Red-Absorbing Ir(III)–Co(III) Dyad, *Inorg. Chem.*, 56 (2017) 10875-10881. doi: 10.1021/acs.inorgchem.7b00684
- [85] M. Wang, Y. Na, M. Gorlov, L. Sun, Light-driven hydrogen production catalysed by transition metal complexes in homogeneous systems, *Dalton Trans.*, 56 (2009) 6458-6467. doi: 10.1039/B903809D
- [86] D. Dolui, S. Khandelwal, P. Majumder, A. Dutta, The odyssey of cobaloximes for catalytic H2 production and their recent revival with enzyme-inspired design, *Chem. Comm.*, 56 (2020) 8166-8181. doi: 10.1039/D0CC03103H

- [87] L. Tong, L. Duan, A. Zhou, R.P. Thummel, First-row transition metal polypyridine complexes that catalyze proton to hydrogen reduction, *Coord. Chem. Rev.*, vol. 402, 2020, pp. 213079. doi: 10.1016/j.ccr.2019.213079
- [88] S.-p. Luo, L. Tang, S.Z. Zhan, A cobalt(II) complex of 2,2-bipyridine, a catalyst for electroand photo-catalytic hydrogen production in purely aqueous media, *Inorg. Chem. Comm.*, 86 (2017) 276-280. doi: 10.1016/J.INOCHE.2017.10.027
- [89] R.M. Kellett, T.G. Spiro, Cobalt(I) porphyrin catalysts of hydrogen production from water, Inorg. Chem. 24 (1985) 2373-2377. doi:10.1021/ic00209a011
- [90] C.H. Lee, D.K. Dogutan, D.G. Nocera, Hydrogen generation by hangman metalloporphyrins, *J. Am. Chem. Soc.* 133 (2011) 8775-8777. doi: 10.1021/ja202136y
- [91] J.L. Alvarez-Hernandez, A.E. Sopchak, K.L. Bren, Buffer pKa Impacts the Mechanism of Hydrogen Evolution Catalyzed by a Cobalt Porphyrin-Peptide *Inorg. Chem.*, 59 (2020) 8061-8069. doi: 10.1021/acs.inorgchem.0c00362
- [92] D.J. Sommer, M.D. Vaughn, B.C. Clark, J. Tomlin, A. Roy, G. Ghirlanda, Reengineering cyt *b*<sub>562</sub> for hydrogen production: A facile route to artificial hydrogenases, *Biochim. Biophys. Acta, Bioenerg.* 1857 (2016) 598-603. doi: 10.1016/j.bbabio.2015.09.001
- [93] M. Bonn, H.J. Bakker, G. Rago, F. Pouzy, J.R. Siekierzycka, A.M. Brouwer, D. Bonn, Suppression of Proton Mobility by Hydrophobic Hydration, *J. Am. Chem. Soc.* 131 (2009) 17070-17071. doi: 10.1021/ja9083094
- [94] Z. Xing, L. Hu, D.S. Ripatti, X. Hu, X. Feng, Enhancing carbon dioxide gas-diffusion electrolysis by creating a hydrophobic catalyst microenvironment, *Nat. Commun.*, 12 (2021) 136. doi: 0.1038/s41467-020-20397-5

[95] R. Alcala-Torano, N. Halloran, N. Gwerder, D.J. Sommer, G. Ghirlanda, Front. in Mol. Biosci. 8 (2021) 609654. doi: 10.3389/fmolb.2021.609654

[96] R.C. Rodrigues, Á. Berenguer-Murcia, D. Carballares, R. Morellon-Sterling, R. Fernandez-Lafuente, Stabilization of enzymes via immobilization: Multipoint covalent attachment and other stabilization strategies, *Biotechnol. Adv.*, 52 (2021) 107821. doi:

10.1016/j.biotechadv.2021.107821

[97] L.J. Perkins, B.R. Weaver, A.R. Buller, J.N. Burstyn, De novo biosynhesis of a nonnatural cobalt porphyrin cofactor in *E. coli* and incorporation into hemoproteins, *PNAS*, 118 (2021) e2017625118. doi: 10.1073/pnas.2017625118